Polymorphic residues in an allelic rice NLR expand binding and response to effectors of the blast pathogen

De la Concepcion JC*[a], Franceschetti M*[a], Maqbool A[a^], Saitoh H[b], Terauchi R[c,d], Kamoun S[e] & Banfield MJ[#a]

[a] Department of Biological Chemistry, John Innes Centre, Norwich Research Park, Norwich, NR4 7UH, UK

[b] Laboratory of Plant Symbiotic and Parasitic Microbes, Department of Molecular Microbiology, Faculty of Life Sciences, Tokyo University of Agriculture, 1-1-1 Sakuragaoka, Setagaya-ku, Tokyo 156-8502, Japan

[c] Division of Genomics and Breeding, Iwate Biotechnology Research Center, Iwate 024-0003, Japan

[d] Laboratory of Crop Evolution, Graduate School of Agriculture, Kyoto University, Kyoto, 606-8501, Japan

[e] The Sainsbury Laboratory, Norwich Research Park, Norwich, NR4 7UH, UK

* These authors contributed equally to this work

^ Current address: The Sainsbury Laboratory, Norwich Research Park, Norwich, NR4 7UH, UK

Corresponding author. Tel: +44 (0)1603 450742, email: mark.banfield@jic.ac.uk

ORCID IDs:

Juan Carlos De la Concepcion: orcid.org/0000-0002-7642-8375

Marina Franceschetti: orcid.org/0000-0002-1389-6825

Abbas Maqbool: orcid.org/0000-0002-6189-5560

Hiromasa Saitoh: orcid.org/0000-0002-0124-9276

Ryohei Terauchi: orcid.org/0000-0002-0095-4651

Sophien Kamoun: orcid.org/0000-0002-0290-0315

Mark J Banfield: orcid.org/0000-0001-8921-3835

Abstract

Accelerated adaptive evolution is a hallmark of plant-pathogen interactions. Plant intracellular immune receptors (NLRs) often occur as allelic series with differential pathogen specificities. The determinants of this specificity remain largely unknown. Here, we unravelled the biophysical and structural basis of expanded specificity in the allelic rice NLR receptor Pik, which responds to the effector AVR-Pik from the rice blast pathogen *Magnaporthe oryzae*. Rice plants expressing the Pikm allele resist infection by blast strains expressing any of three AVR-Pik effector variants, whereas those expressing Pikp only respond to one. Unlike Pikp, the integrated HMA domain of Pikm binds with high affinity to each of the three recognised effector variants, and variation at binding interfaces between effectors and Pikp-HMA/Pikm-HMA domains encodes specificity. By understanding how co-evolution has shaped the response profile of an allelic NLR, we highlight how natural selection drove the emergence of new receptor specificities. This work has implications for engineering of NLRs with improved utility in agriculture.

Introduction

The innate immune systems of plants and animals monitor the extracellular space and intracellular environment for the presence and activities of microbial pathogens[1,2]. In plants, immune receptors of the NLR (nucleotide-binding, leucine-rich repeat) superfamily monitor the intracellular space for signatures of non-self, typically detecting translocated pathogen effector proteins either by direct-binding, or indirectly via monitoring their activity on host targets[3,4]. Co-evolution between pathogens and hosts has driven diversification of plant NLRs, with many NLR genes present in allelic series, with distinct effector recognition profiles[5-15]. Pathogen effectors can show strong signatures of positive selection including high levels of non-synonymous (resulting in amino acid changes) over synonymous polymorphisms[5,7,12,16-18]. How NLR and effector diversification contributes to gene-for-gene immunity in plants is poorly understood. Defining how allelic NLRs recognise and respond to specific pathogen effectors offers new opportunities to engineer control of plant diseases[19,20], leading to improved global food security.

Many NLRs function synergistically, with some acting as a "sensors", to detect pathogens, and others as "helpers", required for initiation of immunity[1,21,22]. These NLRs can be genetically linked in pairs, with a shared promoter[21,23-26], or unlinked but part of a complex genetic network[27]. One mechanism of effector recognition by sensor NLRs is via unconventional integrated domains that likely have their evolutionary origin as host effector targets[28-31]. Such integrated domains can act as "baits" to target effectors by direct binding, or act as substrates of an effector's enzymatic activity[28,31]. Genetically paired NLRs with integrated domains have repeatedly evolved in rice[29,30], and can detect effectors from the rice blast pathogen *Magnaporthe oryzae* (syn. *Pyricularia oryzae*), the causative agent of the most devastating disease of rice - the staple crop that feeds more than half the world population[5,25,26,32].

The rice NLR pair Pik is comprised of Pik-1 (the sensor) and Pik-2 (the helper). This receptor pair responds to the *M. oryzae* effector AVR-Pik by direct binding to an integrated HMA (heavy metal-associated) domain, positioned between the CC (coiled-coil) and nucleotide-binding (NB) domains of Pik-1[33] (**Fig. 1a**). Both the AVR-Pik effectors and the Pik NLRs exist as an allelic series in *M. oryzae* and rice respectively, most likely arisen through co-evolutionary dynamics between pathogen and host[5,34,35]. As such, they represent an excellent system for understanding the mechanistic basis of recognition in plant immunity. Comparison of amino acid sequence identity between the domains of paired Pik NLR alleles shows the integrated HMA domain is the most polymorphic region[35] (**Fig. 1a,c**), consistent with this being the direct binding region for the AVR-Pik effectors. The HMA domain also contains variable amino acids that have been used as a markers for Pik allele identification in rice[35]. In addition, AVR-Pik is a remarkable example of an effector with an extreme signature of positive selection, as all known AVR-Pik nucleotide polymorphisms are non-synonymous, resulting in amino acid changes[16,18] (**Fig. 1b**). Further, these polymorphisms map to

interface residues identified in the crystal structure of the effector variant AVR-PikD bound to the HMA domain of the NLR allele Pikp[33], suggesting they are adaptive.

While rice plants expressing the NLR allele Pikp are resistant to *M. oryzae* strains expressing the effector variant AVR-PikD, rice plants expressing the allele Pikm respond to strains expressing AVR-PikD, AVR-PikE, or AVR-PikA[34] (**Fig. 1b**). Importantly, neither Pikp nor Pikm respond to the stealthy effector variant AVR-PikC, which evades detection by any known Pik NLR[34]. The molecular mechanism by which Pik NLR variation acts to expand effector recognition remains unclear.

Previous work established the structural basis of AVR-PikD recognition by the Pikp-1 NLR[33]. Here, we reveal how co-evolutionary dynamics between a pathogen and a host has driven the emergence of new receptor specificities. By taking advantage of our ability to reconstruct complexes between Pik-HMA domains and AVR-Pik effectors, and to recapitulate cell death responses (indicative of immunity) in the model plant *Nicotiana benthamiana*, we show a correlation between protein binding affinities, and activation of immunity. By obtaining crystal structures of the Pikm-HMA domain in complex with three different AVR-Pik variants, we define the interfaces that support expanded effector recognition. We also obtained new structures of the Pikp-HMA domain in complex with the recognised effector AVR-PikD, but also with the unrecognised AVR-PikE. Together, these structures establish a previously unappreciated role for the C-terminus of the HMA domain in mediating effector interaction. Understanding how host NLRs have evolved new specificities in response to pathogen effectors highlights the potential to engineer new-to-nature receptors with improved functions such as recognition of stealthy effector variants, and has broad implications for rational design of plant NLRs.

Results

Pikm-mediated cell death in *N. benthamiana* recapitulates allele-specific effector responses in rice

Pikp-mediated cell death in *N. benthamiana* phenocopies effector variant-specific resistance in rice, with Pikp responding to AVR-PikD, but not AVR-PikE, AVR-PikA, or AVR-PikC[33]. Here, we show that Pikm responds to each of AVR-PikD, AVR-PikE, or AVR-PikA, but not to AVR-PikC, in this assay (**Fig. 1d,e, Table 1**). These results match the response of rice cultivars expressing Pikm to *M. oryzae* strains encoding the effectors[34]. Interestingly, we observe a qualitative hierarchy in the level of Pikm-mediated cell death in response to the effectors in the order AVR-PikD > AVR-PikE > AVR-PikA (**Fig. 1d,e**). To allow for direct comparison, we repeated this assay using the Pikp NLRs and the effector variants in the same expression vectors. We obtained equivalent results to those shown previously[33] (**Supplementary Fig. 1a,b**). The expression of each protein was confirmed by western blot (**Supplementary Fig. 1c**).

Allele-specific effector responses in planta correlates with direct Pik-HMA interactions

We used yeast-2-hybrid (Y2H) to investigate whether the binding of effectors to the Pikp-HMA domain (henceforth Pikp-HMA) or Pikm-HMA domain (henceforth Pikm-HMA) correlates with in planta response profiles. We observed comparable growth of yeast on selective plates, and the development of blue colouration with X- α-gal (both indicative of protein/protein interactions), with Pikm-HMA and AVR-PikD, AVR-PikE, and AVR-PikA, but not AVR-PikC (**Fig. 2a**). While the Y2H assay with Pikm-HMA or Pikp-HMA showed comparable interaction with AVR-PikD, Pikm-HMA showed increased interaction with AVR-PikE and markedly stronger interaction with AVR-PikA (**Fig. 2a**). No growth was observed with Pikp-HMA and AVR-PikC. All proteins were confirmed to be expressed in yeast (**Supplementary Fig. 2a**).

Pikm-HMA has tighter binding affinities for AVR-Pik effectors compared to Pikp-HMA in vitro

To produce stable Pikm-HMA protein for in vitro studies, we cloned a construct with a 5-amino acid extension at the C-terminus (encompassing residues Gly186 - Asp264 of the full-length protein) compared to the previously studied Pikp-HMA[33]. Using gel filtration with separately purified proteins, Pikm-HMA forms complexes with the effectors AVR-PikD, AVR-PikE, or AVR-PikA, but not with AVR-PikC (**Fig. 2b**, **Supplementary Fig. 2b**).

To determine the extent to which the expanded response of Pikm to AVR-Pik effectors in *N. benthamiana* is related to the strength of binding to the Pikm-HMA, we

determined binding affinities by Surface Plasmon Resonance (SPR). We monitored response units (RU) following Pikm-HMA injection after capturing effectors on the chip surface. Binding of Pikm-HMA to the different effectors was measured at three different concentrations, and RUs normalised to R_{max} (theoretical maximum response, assuming a 1:1 interaction model). From this, we ranked the order of highest to lowest apparent affinity (**Fig. 2c**). We then extended the Pikm-HMA concentration range to enable estimation of the equilibrium dissociation constant, K_D. Using a 1:1 kinetics interaction model, we found that Pikm-HMA bound to AVR-PikD with the highest affinity (lowest K_D), followed by AVR-PikE and AVR-PikA (**Fig. 2c, Supplementary Fig. 2c-e**, **Supplementary Table 1**). We observed no significant binding of Pikm-HMA to AVR-PikC (**Fig. 2c, Supplementary Fig. 2f**, **Supplementary Table 1**).

We also produced Pikp-HMA with its equivalent 5-amino acid C-terminal extension (including residues Gly186 – Asp263 of the full-length protein) and analysed effector binding by SPR (**Fig. 2c**). We ranked effector binding affinities in the order AVR-PikD > AVR-PikE > AVR-PikA (with no significant binding to AVR-PikC, and assuming a 1:2 (effector:Pikp-HMA) interaction model, as previously observed[33]). However, we were only able to reliably determine the K_D for Pikp-HMA bound to AVR-PikD (**Fig. 2c, Supplementary Fig. 2g**), as the binding of AVR-PikE and AVR-PikA were of insufficient quality under our assay conditions to allow K_Ds to be determined (**Supplementary Fig. 2h-i)**.

Based on these results, and the interactions monitored by Y2H, we conclude that differential binding affinity to the HMA domains is the source of the allele-specific response profile in *N. benthamiana*, and of rice cultivars to *M. oryzae* strains expressing AVR-Pik variants[34].

Structures of Pik-HMAs in complex with AVR-Pik effectors reveals multiple interaction surfaces

Using a co-expression strategy, we obtained complexes of Pikm-HMA bound to AVR-PikD, AVR-PikE, or AVR-PikA. Each of these were crystallised, and X-ray diffraction data were collected at the Diamond Light Source (UK) to 1.2 Å, 1.3 Å, and 1.3 Å resolution respectively. Details of X-ray data collection, structure solution, and structure completion are given in the **Methods** and **Supplementary Table 2**. The overall orientations of each component in the Pikm-HMA/effector complexes are similar to each other, and to the previously determined Pikp-HMA/AVR-PikD structure[33] (**Fig. 3a, Supplementary Fig. 3a,b, Supplementary Table 3**). Interestingly, the Pikm-HMA/effector structures form a 1:1 complex, in contrast to Pikp-HMA/AVR-PikD, which formed a 2:1 complex[33]. Pikp-HMA dimerization is most likely an artefact of in vitro protein expression and purification.

Analysis of the interfaces formed between Pikm-HMA and the effectors using QtPISA[36] (**Supplementary Table 4, Supplementary Fig. 4**) reveals they are broadly

similar to each other, although there is a trend of reducing total interface area in the order AVR-PikD > AVR-PikE > AVR-PikA. Graphical representation of key interface components (using QtPISA interaction radars[36], **Supplementary Fig. 4**) reveals a high likelihood that each interface is biologically relevant: each key component value lies well above the 50% threshold when considered against statistical distributions derived from the Protein DataBank (PDB) (see **Methods** and [36]).

Three predominant regions can be identified within each Pikm-HMA/effector interface (**Fig. 3b, Fig. 1c**). These regions (interfaces) are defined here from the HMA side as: interface 1, N-terminal residues Glu188 – Lys191; interface 2, residues from β2 and β3 (Ser219 – Val233), and Lys195 from β1; interface 3, residues from β4 to the C-terminus (Met254 – Asp264) (**Fig. 3b, Fig. 1c**).

Interface 1 is a minor component of the Pikm-HMA/effector interaction, with a single, weak hydrogen bond formed by the side-chain of Lys191 (to the main-chain carbonyl group of Thr69 of the effector), and a hydrophobic interface contributed by the side chain of Met189 (to the side chain of Ile49 of the effector). Interface 2 is more extensive, and predominately interacts with AVR-Pik residues from the N-terminal extension of the conserved MAX effector fold[37], including Arg39 – Phe44 and His46 – Ile49. This interface includes the polymorphic residues at positions 46, 47, and 48 of the effector variants[34] (**Fig. 1b**, **Fig. 3a-d**). Interface 2 also includes salt-bridge/hydrogen bond interactions via the side chains of Asp225 (to Arg64 of the effectors), and Lys195 (to Asp66 of the effectors, **Fig. 3a**). Finally, interface 3 includes both main-chain hydrogen bonding interactions between β4 of the HMA and β3 of the effectors, and inserts the side-chain of Lys262 into a surface pocket on the effector lined by residues Glu53, Tyr71, Ser72, and Trp74. Lys262 makes a number of interactions in this pocket, including salt-bridge/hydrogen bonds with the side-chains of Glu53 and Ser72 (**Fig. 3a, Fig. 4a**).

We also obtained crystal structures of Pikp-HMA, with the 5-amino acid extension at the C-terminus of the HMA, bound to AVR-PikD or AVR-PikE at 1.35 Å and 1.9 Å resolution respectively (see **Methods**, **Supplementary Table 2**, **Supplementary Fig. 3c,d**). The Pikp/AVR-PikE combination does not give rise to responses in planta, but we were able to obtain the complex in solution. The new structure of the Pikp-HMA/AVR-PikD complex is essentially identical to that previously determined[33], except for the 5-amino acid extension. Interface analysis with QtPISA (**Supplementary Table 4**, **Supplementary Fig. 4**) reveals that the Pikp-HMA/AVR-PikD complex has broadly similar properties to those of Pikm-HMA/effectors (total interface area and key component values well above the 50% threshold in interaction radars). In contrast, while the Pikp-HMA/AVR-PikE interface shows a broadly similar total interface area to the other complexes, the total calculated binding energy is reduced (area of the polygon in **Supplementary Fig. 4**), and 5 out of 6 key interface components fall below the 50% threshold, questioning this interface's biological relevance.

Structural changes at interface 2 underpin differential effector recognition by Pikm

Effector variants AVR-PikD, AVR-PikE, and AVR-PikA differ at amino acid positions 46, 47 and 48, which localise to interface 2 (**Fig. 1b, Fig. 3b**). Pikp-HMA binds AVR-PikD(His46) via hydrogen bonds with residues Ser218 and Glu230[33]. In Pikm, the Ser is conserved, but Glu230 is replaced by Val231 at the structurally equivalent position, resulting in the loss of a direct hydrogen bond. Despite this, AVR-PikD(His46) occupies the same position in both complexes (**Fig. 3c**). Surprisingly, in the Pikm-HMA/AVR-PikE complex, AVR-PikE(Asn46) is rotated out of the binding pocket, well away from Val231 (**Fig. 3d**), and a water molecule occupies the resulting space. Hydrogen bonds are formed between AVR-PikE(Asn46:Nδ2) and both Pikm-HMA(Ser219:OH) and the new water molecule. This configuration impacts the position of effector residues Phe44 – Gly48, pushing them away from the HMA, further altering interactions across interface 2. These structural changes correlate with reduced binding affinity of AVR-PikE with Pikm-HMA compared to AVR-PikD. In the Pikm-HMA/AVR-PikA complex, Asn46 is rotated even further out of the HMA pocket, and while a hydrogen bond is still formed with Pikm-HMA(Ser219:OH), this is significantly different in orientation (**Fig. 3d**). These changes serve to move residues Asn46 – Pro50 of AVR-PikA further away from the HMA, and again these structural observations correlate with reduced effector binding affinity. Interestingly, the polymorphic residues in AVR-PikA (Ala47 and Asp48) have no direct role in Pikm-HMA interaction. The polymorphisms in AVR-Pik do not significantly alter protein/protein interactions across interfaces 1 and 3, and these regions appear to stabilise the complexes.

We conclude that the structural changes at interface 2 underlie the weaker binding affinities of Pikm-HMA for AVR-PikE and AVR-PikA, compared to AVR-PikD.

Interactions across interface 3 contribute more to Pikm-HMA than Pikp-HMA binding to AVR-PikD

As observed at interface 3 for the Pikm/effector complexes (**Fig. 4a**), a Lys residue from Pikp-HMA (Lys262) locates to the binding pocket on the effector containing Glu53 and Ser72 (**Fig. 4b**). However, this Lys is shifted one residue to the C-terminus in the sequence of Pikp-1 (**Fig. 1c**). This results in a different conformation of Pikp-HMA residues Ala260 and Asn261 when compared to Pikm-HMA (Val261 and Lys262), changing the interactions across interface 3. The most dramatic difference is the "looping-out" of Pikp-HMA(Asn261), to retain Lys262 in the effector binding pocket (**Fig. 4b, Fig. 5d,e**), which affects the packing of Pikp-HMA(Ala260) (Val261 in Pikm-HMA) and hydrophobic packing of the side-chain of Lys262.

Pik alleles also differ in the composition of residues at interfaces 1 and 2. Of most significance are the changes at interface 2 that contact AVR-PikD(His46), as discussed above and **Fig. 3c**.

We propose that Pikm has evolved more robust interactions across interface 3 compared to Pikp to compensate for loss of binding, such as direct hydrogen bonds, at interface 2.

Interactions across interfaces 2 and 3 underpin specificity of Pikp to AVR-PikD over AVR-PikE

Underpinning the global analysis of the Pikp-HMA/AVR-PikD and Pikp-HMA/AVR-PikE complexes are extensive differences at interfaces 2 and 3. At interface 2, AVR-PikE(Asn46) is fully rotated out of the AVR-PikD(His46) binding pocket (**Fig. 5a-c**). A hydrogen bond is still formed between AVR-PikE(Asn46) and Pikp-HMA(Ser218), but in a very different orientation (**Fig. 5a-c**). This results in residues Asn46-Pro50 moving away from the HMA. This re-configuration is coupled with changes at interface 3 (**Fig. 5d,f,g**). Interestingly, in the Pikp-HMA/AVR-PikE complex, Lys262 adopts a similar orientation to that found in the Pikm-HMA complexes (**Fig. 5e,f,g**). But to enable this, residues Ser258 – Asn261 adopts a dramatically different position, looping-out residues Gln259 and Ala260 from their positions in the Pikm-HMA complex (**Fig. 5e,f,g**), with consequent impacts on this interface.

We conclude that interface 2 is key for effector recognition by Pikp and, unlike for Pikm, interfaces 1 and 3 are not able to compensate to enable productive binding.

Mutations at separate interfaces have differential effects on Pik-HMA/effector interactions and immunity phenotypes

We subsequently tested whether mutations in the effectors at interfaces 2 and 3 have differential effects on Pik-HMA binding and responses by Y2H, SPR and in *N. benthamiana*. We used the previously characterised AVR-PikD(His46Glu) mutant at interface 2, and a Glu53Arg mutant at interface 3 in AVR-PikD, AVR-PikE, and AVR-PikA. While AVR-PikD(His46) occupies a central position at interface 2, AVR-Pik(Glu53) locates to the Pik-HMA(Lys262) binding pocket, at the periphery of interface 3.

As previously observed (although without the C-terminal extension[33]), the AVR-PikD(His46Glu) mutant essentially blocks the Pikp-HMA/effector interaction in Y2H and SPR, and abolishes Pikp-mediated cell death in *N. benthamiana* (**Fig. 6a-c, Supplementary Fig. 5**). Interestingly, AVR-PikD(His46Glu) interacts with Pikm-HMA in Y2H (**Fig. 6a**). However, when measured by SPR, Pikm-HMA binding to this mutant is reduced to ~11% compared to wild-type (**Fig. 6b**). This reduction of binding in vitro is reflected in *N. benthamiana*, where we observe weak AVR-PikD(His46Glu)-dependent Pikm cell death (**Fig. 6c, Supplementary Fig. 5b-d**).

For each of the Glu53Arg effector mutants, we observe little impact on Pikm-HMA interaction in Y2H compared to wild-type, except a reduced interaction of AVR-PikA(Glu53Arg) (**Fig. 6a**). Interestingly, the Glu53Arg mutant in AVR-PikE abolishes interaction of this effector with Pikp-HMA in Y2H. Using SPR, the AVR-Pik(Glu53Arg) mutants show reduced binding to both Pik-HMA domains when compared pairwise with wild-type in each effector background (**Fig. 6b**). However, in each case, the Glu53Arg mutant has a greater effect in Pikm-HMA binding compared to Pikp-HMA. Surprisingly, in the *N. benthamiana* cell death assay, we observe a slight increase in the AVR-PikD(Glu53Arg)-dependent cell death compared to wild-type for both Pikp and Pikm (**Fig. 6c, Supplementary Fig. 5b-d**). However, we see a reduction in intensity of Pikm-mediated cell death for the effector variants AVR-PikE(Glu53Arg) and AVR-PikA(Glu53Arg) (**Fig. 6c, Supplementary Fig. 5b-d**).

We conclude that interactions across interface 2 are critical for effector recognition by Pikp, and important for Pikm, and interface 3 has an important role in the extended response of Pikm to AVR-PikE and AVR-PikA.

Discussion

Despite intensive study, 25 years since the cloning of the first plant NLRs[38-40] very little is known about the molecular mechanistic basis of how these proteins recognise pathogen effectors and initiate immune signalling. The recent identification of plant NLRs with integrated domains[28-30] has enabled new opportunities to investigate how these receptors directly recognise pathogen effectors at the biochemical and structural level, and how these binding events are linked to disease resistance[33,41-44]. Here we have generated five structures of different complexes between the integrated domains of an allelic NLR (Pik), and the variants of the effector (AVR-Pik) they recognise. When combined with analysis of biophysical interactions in vitro, and cell death responses in the model plant *N. benthamiana*, these structures provide new understanding, and unexpected findings, on how co-evolution has driven the emergence of new plant NLR receptor specificities.

High levels of diversifying selection in allelic plant NLRs and pathogen effectors suggest direct interaction between the proteins. Previous studies where structures of the effectors, but not the interacting NLR domain, were available showed that distributed surface-presented residues on the effectors defined NLR recognition specificity, mediated by polymorphic LRR domains[14,15]. The integrated HMA domains are the most polymorphic regions of the rice Pik-1/Pik-2 paired NLRs, and Pik-HMA amino acids that form the interfaces with effectors are likely under the strongest selective pressure. Therefore, during the course of plant-pathogen co-evolution, at least two alternative solutions for recognising divergent effectors have emerged. One of these involves the integration and diversification of non-canonical domains in the NLR architecture. The second involves diversification of LRR domains. An important question raised by these studies is what has driven the emergence of these different systems? An advantage of the integrated domain is that (once stably incorporated) it may tolerate accelerated accumulation of mutations, followed by selection for function, as mutations may be less likely to disrupt to the overall structure and function of the NLRs.

One outcome from this work is the surprising plasticity of the Pik-HMA interfaces that supports differential recognition of AVR-Pik variants. Interactions across interface 2 are important for effector binding by Pikp-HMA and Pikm-HMA. Disruption of interface 2 by amino acid polymorphisms in AVR-PikE and AVR-PikA eliminates Pikp-mediated cell death in planta, and weakens Pikm-mediated cell death. The unique polymorphism that defines AVR-PikC (Ala67Asp) also maps to interface 2, and may result in a steric clash preventing, or severely reducing, Pik-HMA binding. Our structural data support a conclusion that more favourable interactions across interface 3 have evolved in Pikm-HMA to, in-part, compensate for the impact of AVR-Pik variation at interface 2, and support cell-death signalling. Our biophysical data suggest that quantitative binding differences, visualised as disruption of interfaces in the structures, underpins differential effector recognition by Pik-HMAs, and a threshold of binding is required for activation of response in planta. These insights will inform

364 future structure/function studies to address whether rational engineering of Pik-
365 HMA effector-binding interfaces can generate NLR receptors with improved
366 recognition profiles. Ultimately, we must understand how recognition of effectors,
367 through either integrated domains or other mechanisms, results in triggering of
368 immune responses in the context of the full-length proteins and, potentially,
369 oligomeric states.

Methods

Gene cloning

For details of gene cloning, please see **Supplementary Methods**.

Expression and purification of proteins for in vitro binding studies

pOPINM encoding Pikm-HMA or Pikp-HMA was transformed into *E. coli* SHuffle cells[45]. Inoculated cell cultures were grown in auto induction media[46] at 30 °C for 6hr and 18 °C overnight. Cells were harvested and proteins extracted as previously reported[33]. AVR-Pik effectors with a cleavable N-terminal SUMO or MBP tag and a non-cleavable C-terminal 6xHis tag were produced in and purified from *E. coli* SHuffle cells as previously described[33] using either auto induction media[46], or Power Broth (Molecular Dimensions).

Protein concentration of AVR-Pik effectors was determined by absorption at 280 nm using a NanoVue spectrophotometer (GE Lifesciences). Measurements were corrected using the molar extinction coefficient 25,105 M^{-1} cm^{-1}, as calculated by Expasy (http://web.expasy.org/protparam). Due the lack of aromatic residues in Pik-HMA domains, protein concentrations were measured using a Direct Detect® Infrared Spectrometer (Merck).

Co-expression and purification of Pik-HMA/AVR-Pik effectors for crystallisation.

Relevant Pik-HMA domains and AVR-Pik effectors were co-expressed in SHuffle cells following co-transformation of pOPINM:Pik-HMA and pOPINA:AVR-Pik, as previously described[33]. Cells were grown in autoinduction media (supplemented with both carbenicillin and kanamycin), harvested, and processed as described in the **Supplementary Methods**. Protein concentrations were measured by absorbance at 280 nm using a NanoVue spectrophotometer and an extinction coefficient of 25,105 M^{-1} cm^{-1} for Pikm-HMA complexes, and 26,720 M^{-1} cm^{-1} for Pikp-HMA complexes, as calculated by Expasy (http://web.expasy.org/protparam).

Protein:protein interaction: Analytical gel filtration

Pikm-HMA and the AVR-Pik effectors were mixed in a molar ratio of 2:1 and incubated on ice for 60 min. In each case a sample volume of 110 µl was separated at 4°C on a Superdex 75 10/300 size exclusion column (GE Healthcare), pre-equilibrated in buffer B, and at a flow rate of 0.5 ml/min. Fractions of 0.5 ml were collected for analysis by SDS-PAGE. The Superdex 75 10/300 column has a void volume of 7.4 ml and a total volume of 24 ml.

Protein:protein interaction: Surface plasmon resonance

Surface plasmon resonance (SPR) experiments were performed on a Biacore T200 system (GE Healthcare) using an NTA sensor chip (GE Healthcare). All proteins were prepared in SPR running buffer (20 mM HEPES pH 7.5, 860 mM NaCl, 0.1% Tween

20). Details of the cycling conditions are given in the **Supplementary Methods**.

The equilibrium dissociation constants (K_D) for Pikm-HMA binding to AVR-Pik alleles, and Pikp-HMA binding to AVR-PikD, were determined from multicycle kinetics curves using the Biacore T200 BiaEvaluation software (GE Healthcare), with a 1:1 or 2:1 fit model respectively. For the interaction between Pikp-HMA and AVR-PikE and AVR-PikA, and for both Pik-HMAs and the AVR-Pik mutants, it was not possible to accurately determine the K_D due to the insufficient quality of the data. In these cases, the level of binding was expressed as a percentage of the theoretical maximum response (R_{max}) normalized for the amount of ligand immobilized on the chip. SPR data was exported and plotted using Microsoft Excel. Each experiment was repeated a minimum of 3 times, with similar results.

Protein:protein interaction: Yeast-2-hybrid analyses

The Matchmaker® Gold Yeast Two-Hybrid System (Takara Bio USA) was used to detect protein–protein interactions between Pik-HMAs and AVR-Pik effectors. DNA encoding Pik-HMAs in pGBKT7 was co-transformed with either the individual AVR-Pik variants or mutants in pGADT7, into chemically competent *Saccharomyces cerevisiae* Y2HGold cells (Takara Bio, USA). Single colonies grown on selection plates were inoculated in 5 ml of SD$^{-Leu-Trp}$ and grown overnight at 30˚C. Saturated culture was then used to make serial dilutions of OD_{600} 1, 1^{-1}, 1^{-2}, 1^{-3}, respectively. Five µl of each dilution was then spotted on a SD$^{-Leu-Trp}$ plate as a growth control, and also on a SD$^{-Leu-Trp-Ade-His}$ plate containing X-α-gal and aureobasidine, as detailed in the user manual. Plates were imaged after incubation for 60 - 72 hr at 30 ˚C. Each experiment was repeated a minimum of 3 times, with similar results.

To confirm protein expression in yeast, total protein was extracted from transformed colonies by boiling the cells for 10 minutes in LDS Runblue® sample buffer. Samples were centrifugated and the supernatant was subjected to SDS-PAGE prior to western blotting. The resulting membranes were probed with Anti-GAL4 DNA-BD (Sigma) for HMA domains in pGBKT7 and Anti-GAL4 Activation Domain (Sigma) antibodies for AVR-Pik effectors in pGADT7.

***N. benthamiana* cell death assays**

Transient gene-expression in planta was performed by delivering T-DNA constructs with *Agrobacterium tumefaciens* GV3101 strain into 4-week old *N. benthamiana* plants grown at 22–25 °C with high light intensity. Pik-1, Pik-2, AVR-Pik and P19 were mixed at OD_{600} 0.4, 0.4, 0.6 and 0.1, respectively. Detached leaves were imaged at 5 dpi from the abaxial side. Images are representative of three independent experiments, with internal repeats. The cell death index used for scoring is as presented previously[33] (also included in **Supplementary Fig. 1d**). Scoring for all replicas is presented as boxplots, generated using R v3.4.3 (https://www.r-project.org/) and the graphic package ggplot2[47]. The centre line represents the median, box limits are upper and lower

quartiles, whiskers are 1.5x interquartile range, and all data points are represented as dots.

The presence of each protein, as expressed in representative assays, was determined by SDS-PAGE/western blot. For this, leaf tissue was frozen, and ground to fine powder in liquid nitrogen using a pestle and mortar. Leaf powder was mixed with 2 times weight/volume ice-cold extraction buffer (10% glycerol, 25 mM Tris pH 7.5, 1 mM EDTA, 150 mM NaCl, 2% w/v PVPP, 10 mM DTT, 1x protease inhibitor cocktail (Sigma), 0.1% Tween 20 (Sigma)), centrifuged at 4,200g/4 °C for 20-30 min, and the supernatant filtered (0.45 µm).

Crystallization, data collection and structure solution

For crystallization, Pik-HMA/AVR-Pik complexes were concentrated in buffer B (see **Supplementary Methods**). Sitting drop, vapor diffusion crystallization trials were set up in 96 well plates, using an Oryx nano robot (Douglas Instruments, United Kingdom). Plates were incubated at 20°C, and crystals typically appeared after 24 - 48 hours. For data collection, all crystals were harvested from the Morpheus® HT-96 screen (Molecular Dimensions), and snap-frozen in liquid nitrogen. Details of each crystallisation condition are given in the **Supplementary Methods**.

X-ray data sets were collected at the Diamond Light Source (Oxford, UK). The data were processed using the xia2 pipeline[48] and AIMLESS[49], as implemented in CCP4[50]. The structures were solved by molecular replacement using PHASER[51] and the Pikp-HMA/AVR-PikD structure[33]. The final structures were obtained through iterative cycles of manual rebuilding and refinement using COOT[52] and REFMAC5[53], as implemented in CCP4[50]. Structures were validated using the tools provided in COOT and MOLPROBITY[54].

Protein interface analyses

Protein interface analyses were performed using QtPISA[36]. For each complex, one Pik-HMA/AVR-Pik effector assembly was used as a representative example. QtPISA interaction radars[36] were produced using the reference parameter "Total Binding Energy". The area of the polygon indicates the likelihood of the interface to constitute part of a biological assembly (the greater the area the more likely). The scales along the beams compare key interface properties to statistical distributions derived from the Protein Databank. In general, if the radar area is contained within the 50% probability circle then the interface is considered superficial, and its biological relevance is questionable. In cases where the radar area is expanded outside the 50% probability circle, the interface is considered more likely to be significant and biologically relevant[36].

Data availability

The co-ordinates and structure factors have been deposited in the Protein Data Bank with accession codes 6FU9 (Pikm-HMA/AVR-PikD), 6FUB (Pikm-HMA/AVR-PikE), 6FUD (Pikm-HMA/AVR-PikA), 6G10 (Pikp-HMA/AVR-PikD) and 6G11 (Pikp-HMA/AVR-PikE).

Acknowledgements

This work was supported by the BBSRC (grants BB/J00453, BB/P012574, BB/M02198X), the ERC (proposal 743165), the John Innes Foundation, the Gatsby Charitable Foundation, and JSPS KAKENHI 15H05779. We thank the Diamond Light Source, UK (beamlines I03 and I04 under proposals MX9475 and MX13467) for access to X-ray data collection facilities. We also thank David Lawson and Clare Stevenson (JIC X-ray Crystallography/Biophysical Analysis Platform) for help with protein structure determination and SPR.

Figures

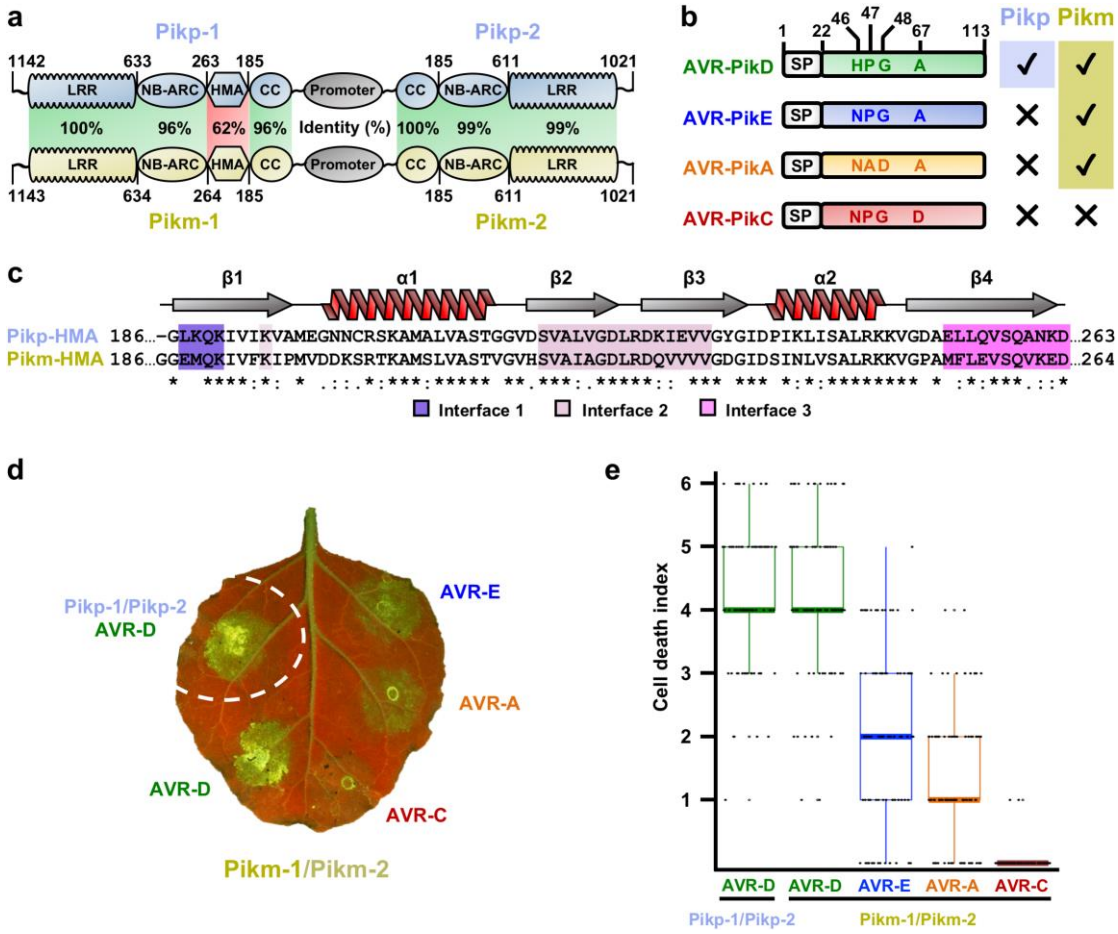

Figure 1: The Pikm-mediated cell death response to AVR-Pik effector variants in *N. benthamiana* phenocopies the Pikm resistance profile in rice. (a) Schematic representations of Pik NLR alleles. The sensor NLR (Pik-1) and helper NLR (Pik-2) share a common promoter and the same overall domain architecture. Pikp-1/Pikp-2 (top) are shown in ice blue, and Pikm-1/Pikm-2 (bottom) are shown in gold. Pairwise protein sequence identity between each domain is indicated, highlighting diversification of the integrated HMA domain, **(b)** Schematic representations of AVR-Pik variants with amino acid polymorphisms shown (single letter code, SP = Signal Peptide), along with their Pikp- or Pikm-mediated response profiles in rice[34], **(c)** Amino acid sequence alignment of Pikp-1 and Pikm-1 HMA domains. Secondary structure features of the HMA fold are shown above, and the residues located to the interfaces described in the text and **Figure 3** are highlighted in purple (interface 1), pink (interface 2), and magenta (interface 3), **(d)** Representative leaf image showing Pikm-mediated cell death to AVR-Pik variants as autofluorescence under UV-light, Pikp-mediated cell death with AVR-PikD is included as a positive control (surrounded by dashed circle, no Pikm-1/Pikm-2 in this spot), **(e)** Box-plots showing repeats of the cell death assay, for each sample the number of repeats was 90. The cell-death scoring scale used is shown in **Supplementary Fig. 1d**. For brevity, effectors are labelled without the 'Pik' designation in panels **(d)** and **(e)** and, where appropriate, in **Figs. 2 – 6**.

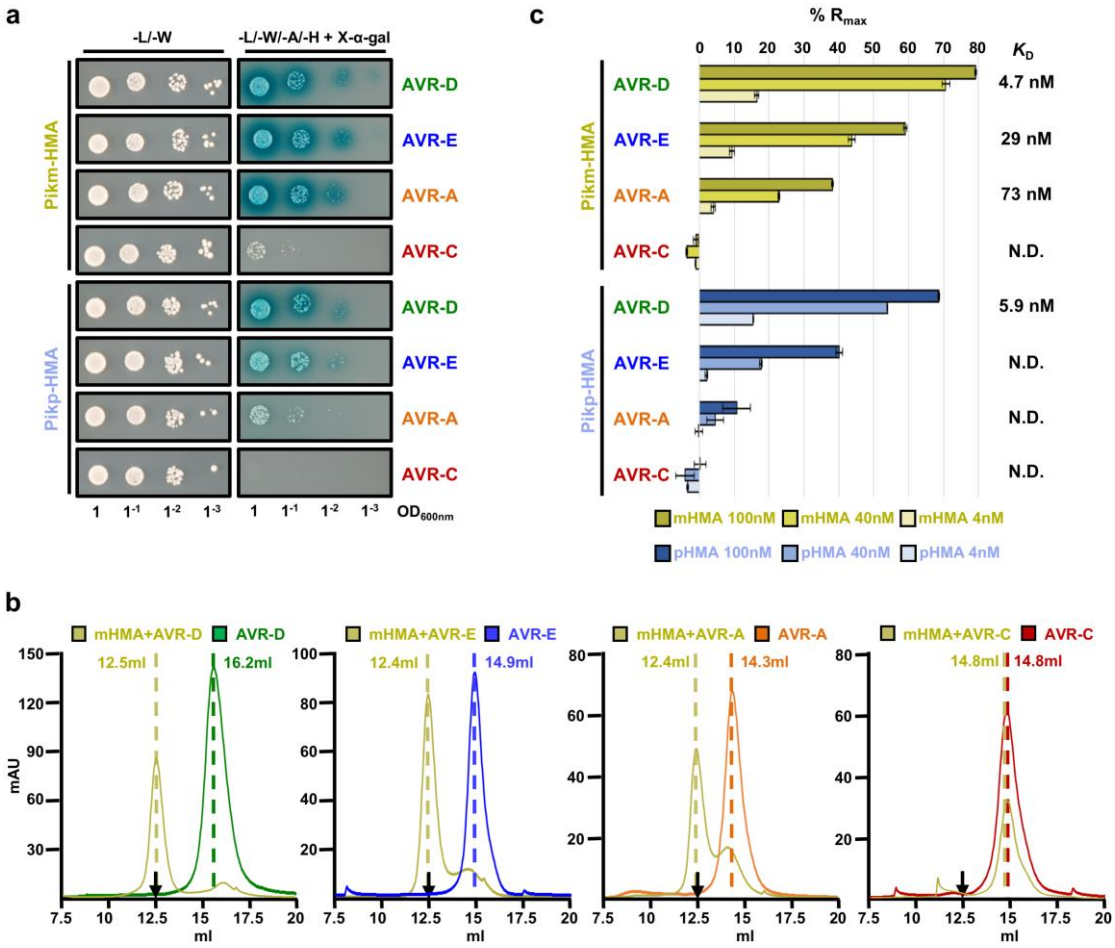

Figure 2: Different affinities underpin recognition and response of Pik NLR alleles to AVR-Pik effector variants. (a) Yeast-2-hybrid demonstrates binding of effector variants to both the Pikm- and Pikp-HMA domains, control plate for yeast growth is on the left, with selective plate on the right, **(b)** Analytical gel filtration confirms that Pikm-HMA forms complexes with AVR-PikD, AVR-PikE, and AVR-PikA in vitro, but not AVR-PikC. Note that earlier elution correlates with increased molecular mass. Retention volumes for peaks are labelled (black arrow indicates Pikm-HMA elution volume, Pikm-HMA does not absorb light at 280 nm). SDS-PAGE with relevant fractions are shown in **Supplementary Fig. 2b**. **(c)** Surface Plasmon Resonance (SPR) reveals in vitro binding affinity between Pik-HMA domains and effectors correlates with in planta responses. $\%R_{max}$ is the percentage of the theoretical maximum response, assuming a 1:1 binding model for Pikm (effector:HMA), and a 1:2 binding model for Pikp, at the HMA concentrations shown. Bars represent the average of 3 measurements, with corresponding standard deviation. Where K_D values are given, a wider range of HMA concentrations were used for this calculation (see **Supplementary Fig. 2c-e, g**), N.D. = Not Determined.

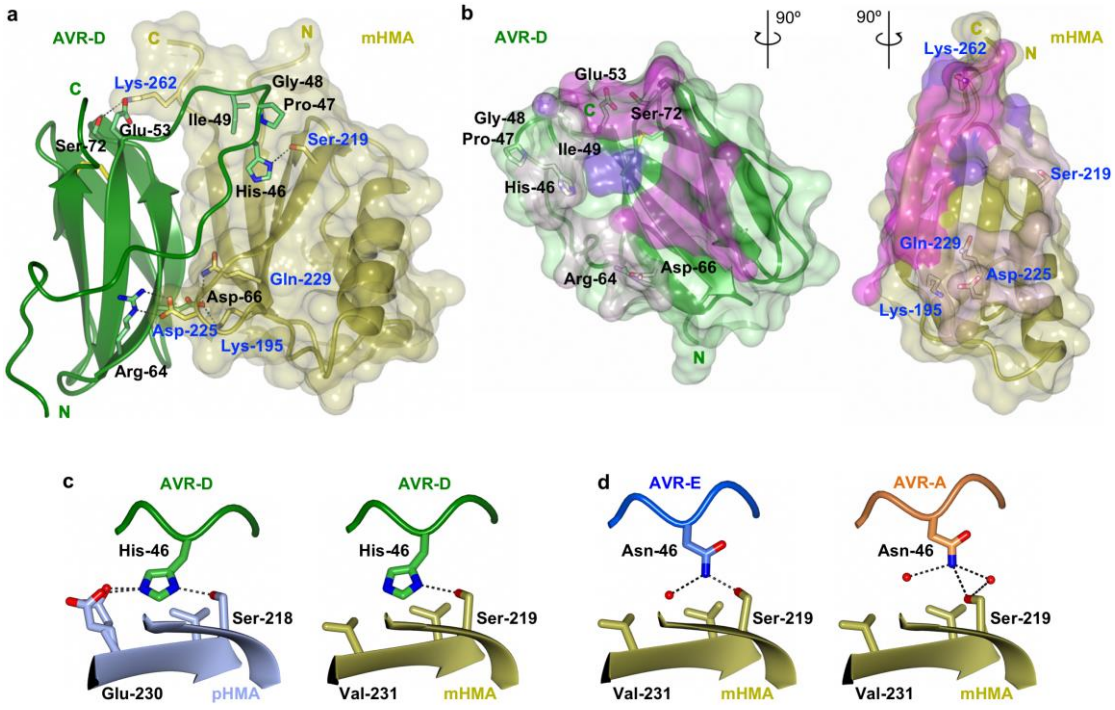

Figure 3: Structures of Pikm-HMA in complex with AVR-Pik effectors. (a) Schematic representation of the structure of Pikm-HMA in complex with AVR-PikD. Pikm-HMA is shown in gold cartoon representation with selected side chains as sticks; the molecular surface of this domain is also shown. AVR-PikD is shown in green cartoon, with selected side chains as sticks. Hydrogen bonds/salt bridges are shown as dashed lines and the di-sulfide bond as yellow bars, **(b)** Buried surface area of AVR-PikD and Pikm-HMA shown from the perspective of the partner (change in orientation from panel (**a**) indicated). The buried surfaces are coloured according to interfaces described in the text (interface 1 is in purple, interface 2 is in pink, interface 3 is magenta), **(c)** Close-up views (part of interface 2) of the orientation and interactions of AVR-PikD(His46) in the Pikp-HMA and Pikm-HMA complexes, **(d)** Close-up views (part of interface 2) of the orientation and interactions of AVR-PikE(Asn46), left, and AVR-PikA(Asn46), right, in complex with Pikm-HMA. Water molecules are shown as red spheres.

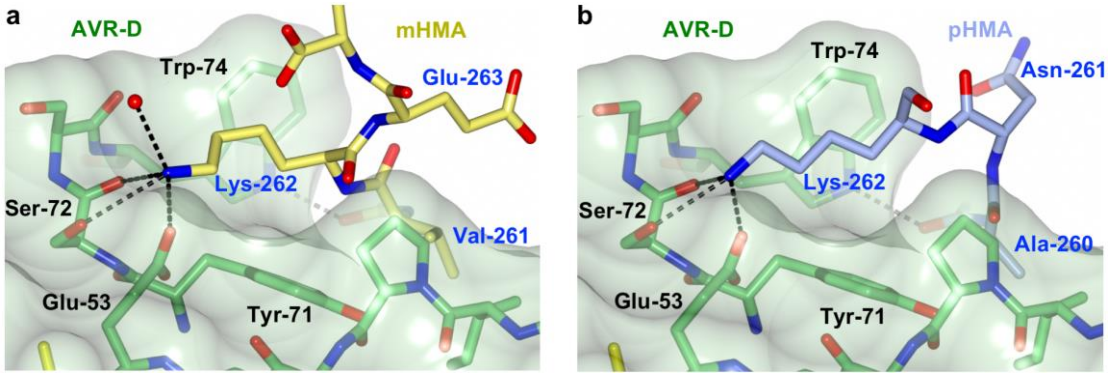

Figure 4: Different interactions at interface 3 in the complexes of Pikm-HMA and Pikp-HMA with AVR-PikD support recognition and response. Close-up view of the interactions across interface 3 in the **(a)** Pikm-HMA and **(b)** Pikp-HMA complexes with AVR-PikD, showing different conformations for the C-terminal regions of the HMA domains. In particular, note the looping-out of Asn261 of Pikp-HMA, and the different orientation of the Lys262 sidechain. In each panel, AVR-PikD is shown in green cartoon, with side chains as sticks, the molecular surface of the effector is also shown. The Pik-HMA domains are coloured as labelled.

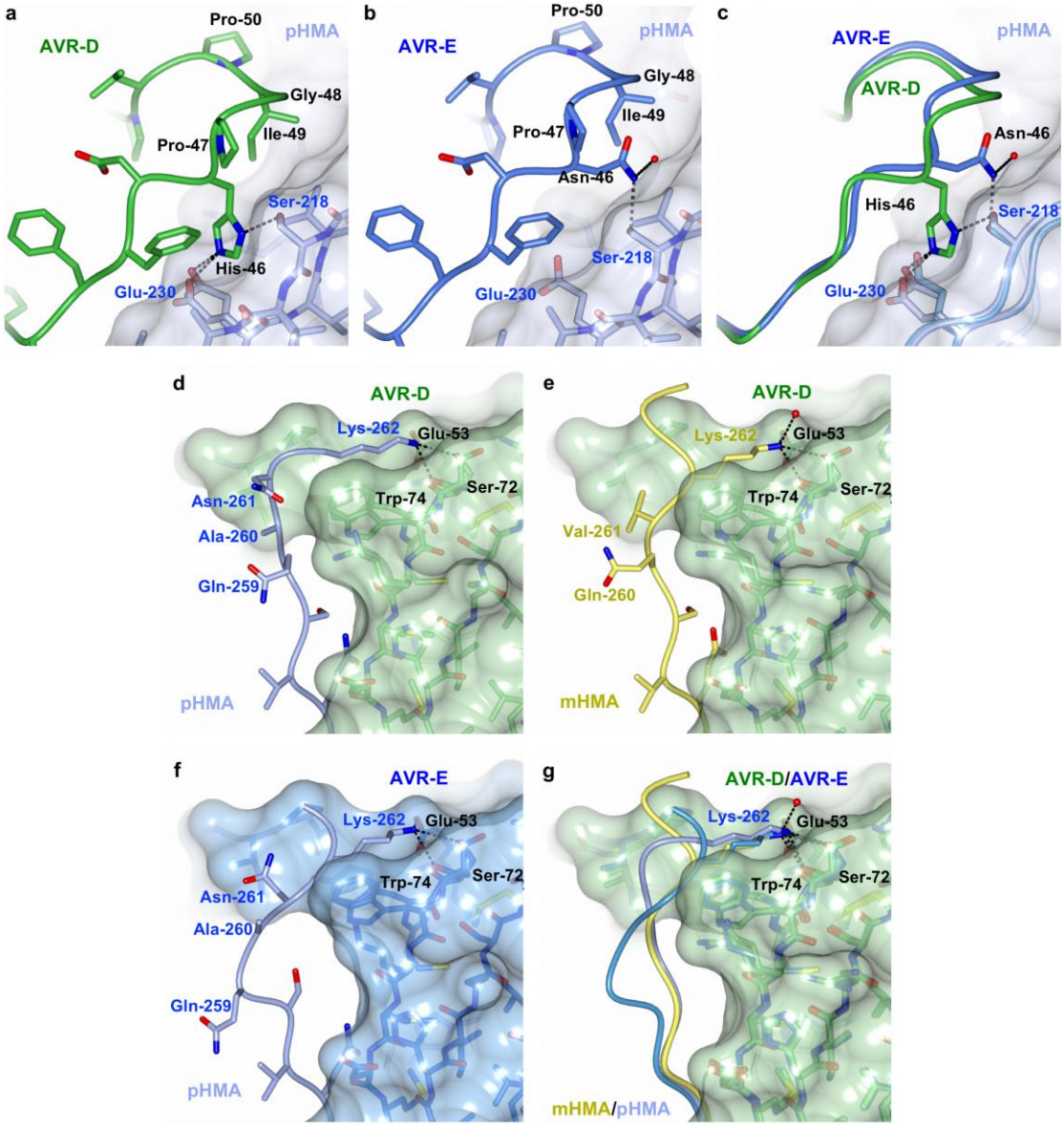

Figure 5: Altered interactions across interfaces of Pikp-HMA with AVR-PikD and with AVR-PikE underpin differences in recognition and response. (a, b) Zoom-in views of the interactions across interface 2 in the Pikp-HMA complexes with AVR-PikD and AVR-PikE. In each panel the Pikp-HMA domain is shown as ice-blue sticks, the molecular surface is also shown. Effector variant residues are coloured as labelled and shown in Cα-worm with sidechain representation, **(c)** Superposition of panels **(a)** and **(b)**, with only selected sidechains shown for clarity. The polymorphism at position 46 occupies a very different position, fully flipped out of the His46 binding pocket in the AVR-PikE structure, which alters the position of residues Asn44-Pro50 relative to the Pikp-HMA domain, **(d-f)** Zoom-in views of the interactions across interface 3 in the Pikp-HMA complex with AVR-PikD, Pikm-HMA complex with AVR-PikD, and Pikp-HMA with AVR-PikE. In each panel the effector is shown as sticks, and the molecular surface is also shown and coloured as labelled. Pik-HMA residues are coloured as labelled and shown in Cα-worm with sidechain representation. The

looping-out of Asn261 in Pikp compared to Pikm, when in complex with AVR-PikD, is seen in panels **d** and **e**, and the displacement of residues Gln259 and Ala260 in Pikp, between the complexes with AVR-PikD or AVR-PikE, is seen in panels **d** and **f**, **(g)** Superposition of panels **(d-f)**, with only the sidechain of Pik-HMA Lys262, and only the surface of AVR-PikD, shown for clarity.

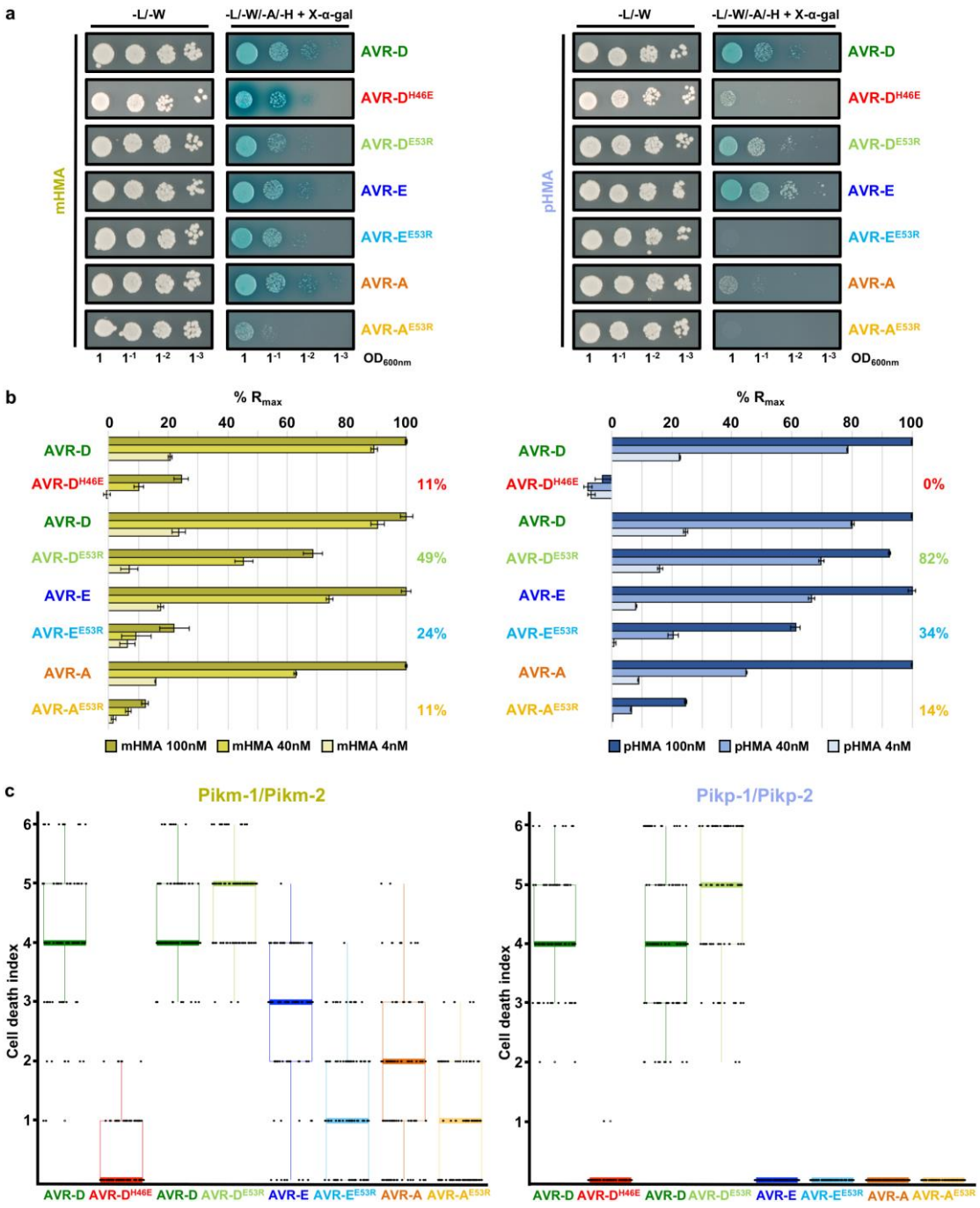

Figure 6: Mutations at different interfaces in the Pik-HMA/effector complexes have differential effects on interactions and phenotypes. (a) Effector mutations at positions 46 and 53 perturb interactions with Pikm- and Pikp-HMA domains as assayed by Y2H, **(b)** Changes in in vitro binding for effector mutants with Pikm- and Pikp-HMA domains, as measured by SPR. $\%R_{max}$ was calculated as described in the text. To emphasise the altered binding for each effector mutant, the averaged difference $\%\ R_{max}$, across the 3 different concentrations measured, is shown. Bars represent the average of 3 measurements, with corresponding standard deviation **(c)**

592 Box-plots of Pikm- or Pikp-mediated cell death triggered by the effector mutants, for
593 each sample the number of repeats was 90.

Table 1: Summary Table detailing the various interactions and phenotypes between Pik NLR alleles and effector variants in this study.

		AVR-D	AVR-E	AVR-A	AVR-C	AVR-D^{H46E}	AVR-D^{E53R}	AVR-E^{E53R}	AVR-A^{E53R}
Interaction in Y2H	Pikp	+++	++	+	-	+	++	-	-
	Pikm	+++	+++	+++	+	+++	++	++	+
Interaction in SPR	Pikp	+++	++	+	-	-	+++	+	-
	Pikm	+++	+++	++	-	+	++	+	-/+
Recognition in rice plants	Pikp	+++*	+*	(-)	(-)	-*	N.D.	N.D.	N.D.
	Pikm	(+++)	(+++)	(+++)	(-)	N.D.	N.D.	N.D.	N.D.
CD response in N. *benthamiana*	Pikp	+++	-	-	-	-	+++	-	-
	Pikm	+++	++	+	-	+	+++	+	+

Y2H = yeast-2-hybrid, SPR = Surface Plasmon Resonance, Recognition in rice plant Pikp = rice cv. K60, Pikm= rice cv. Tsuyuake, CD = cell death, N.D. not determined, parenthesis from[34], *from[33]. SPR and Y2H interactions used the isolated HMA domains, *in planta* experiments were performed with full length proteins.

References

1 Jones, J. D., Vance, R. E. & Dangl, J. L. Intracellular innate immune surveillance devices in plants and animals. *Science* **354**, doi:10.1126/science.aaf6395 (2016).

2 Ronald, P. C. & Beutler, B. Plant and animal sensors of conserved microbial signatures. *Science* **330**, 1061-1064, doi:10.1126/science.1189468 (2010).

3 Dodds, P. N. & Rathjen, J. P. Plant immunity: towards an integrated view of plant-pathogen interactions. *Nat Rev Genet* **11**, 539-548, doi:10.1038/nrg2812 (2010).

4 Win, J. *et al.* Effector Biology of Plant-Associated Organisms: Concepts and Perspectives. *Cold Spring Harb Symp Quant Biol* **77**, 235-247, doi:doi:10.1101/sqb.2012.77.015933 (2012).

5 Bialas, A. *et al.* Lessons in Effector and NLR Biology of Plant-Microbe Systems. *Mol Plant Microbe Interact* **31**, 34-45, doi:10.1094/MPMI-08-17-0196-FI (2017).

6 Ellis, J. G., Lawrence, G. J., Luck, J. E. & Dodds, P. N. Identification of regions in alleles of the flax rust resistance gene L that determine differences in gene-for-gene specificity. *Plant Cell* **11**, 495-506 (1999).

7 Allen, R. L. *et al.* Host-parasite coevolutionary conflict between Arabidopsis and downy mildew. *Science* **306**, 1957-1960, doi:10.1126/science.1104022 (2004).

8 Bhullar, N. K., Zhang, Z., Wicker, T. & Keller, B. Wheat gene bank accessions as a source of new alleles of the powdery mildew resistance gene Pm3: a large scale allele mining project. *BMC Plant Biol* **10**, 88, doi:10.1186/1471-2229-10-88 (2010).

9 Seeholzer, S. *et al.* Diversity at the Mla powdery mildew resistance locus from cultivated barley reveals sites of positive selection. *Mol Plant Microbe Interact* **23**, 497-509, doi:10.1094/MPMI-23-4-0497 (2010).

10 Srichumpa, P., Brunner, S., Keller, B. & Yahiaoui, N. Allelic series of four powdery mildew resistance genes at the Pm3 locus in hexaploid bread wheat. *Plant Physiol* **139**, 885-895, doi:10.1104/pp.105.062406 (2005).

11 Lu, X. *et al.* Allelic barley MLA immune receptors recognize sequence-unrelated avirulence effectors of the powdery mildew pathogen. *Proc Natl Acad Sci U S A* **113**, E6486-E6495, doi:10.1073/pnas.1612947113 (2016).

12 Dodds, P. N. *et al.* Direct protein interaction underlies gene-for-gene specificity and coevolution of the flax resistance genes and flax rust avirulence genes. *Proc Natl Acad Sci U S A* **103**, 8888-8893, doi:10.1073/pnas.0602577103 (2006).

13 Krasileva, K. V., Dahlbeck, D. & Staskawicz, B. J. Activation of an Arabidopsis resistance protein is specified by the in planta association of its leucine-rich repeat domain with the cognate oomycete effector. *Plant Cell* **22**, 2444-2458, doi:10.1105/tpc.110.075358 (2010).

14 Steinbrenner, A. D., Goritschnig, S. & Staskawicz, B. J. Recognition and activation domains contribute to allele-specific responses of an Arabidopsis NLR receptor to an oomycete effector protein. *PLoS Pathog* **11**, e1004665, doi:10.1371/journal.ppat.1004665 (2015).

15 Wang, C. I. *et al.* Crystal structures of flax rust avirulence proteins AvrL567-A and -D reveal details of the structural basis for flax disease resistance specificity. *Plant Cell* **19**, 2898-2912, doi:10.1105/tpc.107.053611 (2007).

16 Huang, J., Si, W., Deng, Q., Li, P. & Yang, S. Rapid evolution of avirulence genes in rice blast fungus Magnaporthe oryzae. *BMC Genet* **15**, 45, doi:10.1186/1471-2156-15-45 (2014).

17 Raffaele, S. *et al.* Genome evolution following host jumps in the Irish potato famine pathogen lineage. *Science* **330**, 1540-1543, doi:10.1126/science.1193070 (2010).

18 Yoshida, K. *et al.* Association genetics reveals three novel avirulence genes from the rice blast fungal pathogen Magnaporthe oryzae. *Plant Cell* **21**, 1573-1591, doi:10.1105/tpc.109.066324 (2009).

19 Dangl, J. L., Horvath, D. M. & Staskawicz, B. J. Pivoting the plant immune system from dissection to deployment. *Science* **341**, 746-751, doi:10.1126/science.1236011 (2013).

20 Rodriguez-Moreno, L., Song, Y. & Thomma, B. P. Transfer and engineering of immune receptors to improve recognition capacities in crops. *Curr Opin Plant Biol* **38**, 42-49, doi:10.1016/j.pbi.2017.04.010 (2017).

21 Eitas, T. K. & Dangl, J. L. NB-LRR proteins: pairs, pieces, perception, partners, and pathways. *Curr Opin Plant Biol* **13**, 472-477, doi:10.1016/j.pbi.2010.04.007 (2010).

22 Wu, C. H., Belhaj, K., Bozkurt, T. O., Birk, M. S. & Kamoun, S. Helper NLR proteins NRC2a/b and NRC3 but not NRC1 are required for Pto-mediated cell death and resistance in Nicotiana benthamiana. *New Phytol* **209**, 1344-1352, doi:10.1111/nph.13764 (2016).

23 Narusaka, M. *et al.* RRS1 and RPS4 provide a dual Resistance-gene system against fungal and bacterial pathogens. *Plant J* **60**, 218-226, doi:10.1111/j.1365-313X.2009.03949.x (2009).

24 Sinapidou, E. *et al.* Two TIR:NB:LRR genes are required to specify resistance to Peronospora parasitica isolate Cala2 in Arabidopsis. *Plant J* **38**, 898-909, doi:10.1111/j.1365-313X.2004.02099.x (2004).

25 Ashikawa, I. *et al.* Two adjacent nucleotide-binding site-leucine-rich repeat class genes are required to confer Pikm-specific rice blast resistance. *Genetics* **180**, 2267-2276, doi:10.1534/genetics.108.095034 (2008).

26 Lee, S. K. *et al.* Rice Pi5-mediated resistance to Magnaporthe oryzae requires the presence of two coiled-coil-nucleotide-binding-leucine-rich repeat genes. *Genetics* **181**, 1627-1638, doi:10.1534/genetics.108.099226 (2009).

27 Wu, C. H. *et al.* NLR network mediates immunity to diverse plant pathogens. *Proc Natl Acad Sci U S A* **114**, 8113-8118, doi:10.1073/pnas.1702041114 (2017).

28 Cesari, S., Bernoux, M., Moncuquet, P., Kroj, T. & Dodds, P. N. A novel conserved mechanism for plant NLR protein pairs: the "integrated decoy" hypothesis. *Front Plant Sci* **5**, 606, doi:10.3389/fpls.2014.00606 (2014).

29 Kroj, T., Chanclud, E., Michel-Romiti, C., Grand, X. & Morel, J. B. Integration of decoy domains derived from protein targets of pathogen effectors into plant immune receptors is widespread. *New Phytol* **210**, 618-626, doi:10.1111/nph.13869 (2016).

30 Sarris, P. F., Cevik, V., Dagdas, G., Jones, J. D. & Krasileva, K. V. Comparative analysis of plant immune receptor architectures uncovers host proteins likely targeted by pathogens. *BMC Biol* **14**, 8, doi:10.1186/s12915-016-0228-7 (2016).

31 Wu, C. H., Krasileva, K. V., Banfield, M. J., Terauchi, R. & Kamoun, S. The "sensor domains" of plant NLR proteins: more than decoys? *Front Plant Sci* **6**, 134, doi:10.3389/fpls.2015.00134 (2015).

32 Okuyama, Y. *et al.* A multifaceted genomics approach allows the isolation of the rice Pia-blast resistance gene consisting of two adjacent NBS-LRR protein genes. *Plant J* **66**, 467-479, doi:10.1111/j.1365-313X.2011.04502.x (2011).

33 Maqbool, A. *et al.* Structural basis of pathogen recognition by an integrated HMA domain in a plant NLR immune receptor. *Elife* **4**, doi:10.7554/eLife.08709 (2015).

34 Kanzaki, H. *et al.* Arms race co-evolution of Magnaporthe oryzae AVR-Pik and rice Pik genes driven by their physical interactions. *Plant J* **72**, 894-907, doi:10.1111/j.1365-313X.2012.05110.x (2012).

35 Costanzo, S. & Jia, Y. L. Sequence variation at the rice blast resistance gene Pi-km locus: Implications for the development of allele specific markers. *Plant Sci* **178**, 523-530, doi:10.1016/j.plantsci.2010.02.014 (2010).

36 Krissinel, E. Stock-based detection of protein oligomeric states in jsPISA. *Nucleic Acids Res* **43**, W314-319, doi:10.1093/nar/gkv314 (2015).

37 de Guillen, K. *et al.* Structure Analysis Uncovers a Highly Diverse but Structurally Conserved Effector Family in Phytopathogenic Fungi. *PLoS Pathog* **11**, e1005228, doi:10.1371/journal.ppat.1005228 (2015).

38 Bent, A. F. *et al.* RPS2 of Arabidopsis thaliana: a leucine-rich repeat class of plant disease resistance genes. *Science* **265**, 1856-1860 (1994).

39 Mindrinos, M., Katagiri, F., Yu, G. L. & Ausubel, F. M. The A. thaliana disease resistance gene RPS2 encodes a protein containing a nucleotide-binding site and leucine-rich repeats. *Cell* **78**, 1089-1099 (1994).

40 Whitham, S. *et al.* The product of the tobacco mosaic virus resistance gene N: similarity to toll and the interleukin-1 receptor. *Cell* **78**, 1101-1115 (1994).

41 Le Roux, C. *et al.* A receptor pair with an integrated decoy converts pathogen disabling of transcription factors to immunity. *Cell* **161**, 1074-1088, doi:10.1016/j.cell.2015.04.025 (2015).

42 Sarris, P. F. *et al.* A Plant Immune Receptor Detects Pathogen Effectors that Target WRKY Transcription Factors. *Cell* **161**, 1089-1100, doi:10.1016/j.cell.2015.04.024 (2015).

43 Zhang, Z. M. *et al.* Mechanism of host substrate acetylation by a YopJ family effector. *Nat Plants* **3**, 17115, doi:10.1038/nplants.2017.115 (2017).

44 Ortiz, D. *et al.* Recognition of the Magnaporthe oryzae Effector AVR-Pia by the Decoy Domain of the Rice NLR Immune Receptor RGA5. *Plant Cell* **29**, 156-168, doi:10.1105/tpc.16.00435 (2017).

45 Lobstein, J. *et al.* SHuffle, a novel Escherichia coli protein expression strain capable of correctly folding disulfide bonded proteins in its cytoplasm. *Microb Cell Fact* **11**, 56, doi:10.1186/1475-2859-11-56 (2012).

46 Studier, F. W. Protein production by auto-induction in high density shaking cultures. *Protein Expr Purif* **41**, 207-234 (2005).

47 Wickham, H. *ggplot. Elegant Graphics for Data Analysis*. (Springer-Verlag New York, 2009).

48 Winter, G. xia2: an expert system for macromolecular crystallography data reduction. *Journal of Applied Crystallography* **43**, 186-190, doi:10.1107/S0021889809045701 (2010).

49 Evans, P. R. & Murshudov, G. N. How good are my data and what is the resolution? *Acta Crystallogr D* **69**, 1204-1214, doi:10.1107/S0907444913000061 (2013).

50 Winn, M. D. *et al.* Overview of the CCP4 suite and current developments. *Acta Crystallogr D Biol Crystallogr* **67**, 235-242, doi:10.1107/S0907444910045749 (2011).

51 McCoy, A. J. *et al.* Phaser crystallographic software. *J Appl Crystallogr* **40**, 658-674, doi:10.1107/S0021889807021206 (2007).

52 Emsley, P., Lohkamp, B., Scott, W. G. & Cowtan, K. Features and development of Coot. *Acta Crystallogr D Biol Crystallogr* **66**, 486-501, doi:10.1107/S0907444910007493 (2010).

53 Murshudov, G. N. *et al.* REFMAC5 for the refinement of macromolecular crystal structures. *Acta Crystallogr D Biol Crystallogr* **67**, 355-367, doi:10.1107/S0907444911001314 (2011).

54 Chen, V. B. *et al.* MolProbity: all-atom structure validation for macromolecular crystallography. *Acta Crystallogr D Biol Crystallogr* **66**, 12-21, doi:10.1107/S0907444909042073 (2010).

747